applied sciences

MDPI

Article

Dual Band Antenna Design and Prediction of Resonance Frequency Using Machine Learning Approaches

Md. Ashraful Haque [1,2], Nayan Sarker [3,*], Narinderjit Singh Sawaran Singh [4], Md Afzalur Rahman [2], Md. Nahid Hasan [2], Mirajul Islam [5], Mohd Azman Zakariya [1], Liton Chandra Paul [6], Adiba Haque Sharker [2], Ghulam E. Mustafa Abro [7], Md Hannan [8] and Ripon Pk [2]

1 Department of Electrical and Electronic Engineering, Universiti Teknologi PETRONAS, Bandar Seri Iskandar 32610, Perak, Malaysia
2 Department of Electrical and Electronic Engineering, Daffodil International University, Dhaka 1341, Bangladesh
3 Department of Electrical and Electronic Engineering, Jatiya Kabi Kazi Nazrul Islam University, Mymensingh 2220, Bangladesh
4 Faculty of Data Science and Information Technology, INTI International University, Persiaran Perdana BBN, Putra Nilai, Nilai 71800, Negeri Sembilan, Malaysia
5 Department of Computer Science and Engineering, Daffodil International University, Dhaka 1341, Bangladesh
6 Department of Electrical, Electronic and Communication Engineering, Pabna University of Science and Technology, Pabna 6600, Bangladesh
7 Condition Monitoring Systems Lab, NCRA, Mehran University of Engineering and Technology, Jamshoro 67480, Pakistan
8 Department of Computer Science and Engineering, City University, Dhaka 1343, Bangladesh
* Correspondence: nayan_ece09@yahoo.com

Citation: Haque, M.A.; Sarker, N.; Sawaran Singh, N.S.; Rahman, M.A.; Hasan, M.N.; Islam, M.; Zakariya, M.A.; Paul, L.C.; Sharker, A.H.; Abro, G.E.M.; et al. Dual Band Antenna Design and Prediction of Resonance Frequency Using Machine Learning Approaches. *Appl. Sci.* **2022**, *12*, 10505. https://doi.org/10.3390/app122010505

Academic Editor: Hosung Choo

Received: 2 September 2022
Accepted: 4 October 2022
Published: 18 October 2022

Abstract: An inset fed-microstrip patch antenna (MPA) with a partial ground structure is constructed and evaluated in this paper. This article covers how to evaluate the performance of the designed antenna by using a combination of simulation, measurement, creation of the RLC equivalent circuit model, and the implementation of machine learning approaches. The MPA's measured frequency range is 7.9–14.6 GHz, while its simulated frequency range is 8.35–14.25 GHz in CST microwave studio (CST MWS) 2018. The measured and simulated bandwidths are 6.7 GHz and 5.9 GHz, respectively. The antenna substrate is composed of FR-4 Epoxy, which has a dielectric constant of 4.4 and a loss tangent of 0.02. The equivalent model of the proposed MPA is developed by using an advanced design system (ADS) to compare the resonance frequencies obtained by using CST. In addition, the measured return loss of the prototype is compared with the simulated return loss observed by using CST and ADS. At the end, 86 data samples are gathered through the simulation by using CST MWS, and seven machine learning (ML) approaches, such as convolutional neural network (CNN), linear regression (LR), random forest regression (RFR), decision tree regression (DTR), lasso regression, ridge regression, and extreme gradient boosting (XGB) regression, are applied to estimate the resonant frequency of the patch antenna. The performance of the seven ML models is evaluated based on mean square error (MSE), mean absolute error (MAE), root mean square error (RMSE), and variance score. Among the seven ML models, the prediction result of DTR (MSE = 0.71%, MAE = 5.63%, RMSE = 8.42%, and var score = 99.68%) is superior to other ML models. In conclusion, the proposed antenna is a strong contender for operating at the entire X-band and lower portion of the Ku-band frequencies, as evidenced by the simulation results through CST and ADS, it measured and predicted results using machine learning approaches.

Keywords: microstrip patch antenna; X-band; machine learning; convolutional neural network; frequency prediction

1. Introduction

Antennas are rightfully referred to as the electronic eyes and ears of the planet because of their unquestionable significance in wireless communication technology [1]. Microstrip patch antennas (MPAs) have been one of the most revolutionary breakthroughs in the time of downsizing in the ever-growing field of wireless communication technology [2,3]. Due to their low weight, miniature size, affordability, ease of fabrication, and ability to be printed directly onto circuit boards, they have been widely used in various wireless systems, such as airborne radar, radio telemetry, RFID, mobile communication, navigation systems, and satellite communication [4,5]. In [6,7], meta surface-based dual band antennas were investigated, especially for industrial, scientific, and medical (ISM) applications. When the incident angles theta and phi change from −90 to 90 and from 0 to 360 degrees, the unit "1" reflection coefficient amplitude changes from 0 to 1. A genetic algorithm (GA) optimizes CFMS coding subarray distribution [6]. The S_{11} of the antenna is less than −10 dB between 2.3–2.62 GHz and 4.9–6.45 GHz and 13% and 27% impedance bandwidth. Additionally, 6.8 dB at 2.45 GHz and 9.0 dB at 5.8 GHz [7]. However, the bandwidth and gain of typical microstrip antennas are both low [8,9], despite their many advantages. Recently, MPAs have been extensively used in X-band applications. An X-band antenna can have both the compact size and the huge bandwidth required to send big data [10,11]. To increase MPA performance and eliminate numerous drawbacks in the X-band range, substantial research work was conducted accordingly [12–17]. A tuning fork-shaped MPA having resonance frequencies ranging from 9 GHz to 11 GHz for X-band radar and satellite applications was presented in [18]. The substrate of Rogers RT/Duroid 5880 in a high-frequency structural simulator (HFSS) simulates and analyzes the antenna characteristics. With total dimensions of 24 × 18 × 1.57 mm^3, the result generated a maximum gain of 5.3 dB. A series-fed microstrip array antenna was also proposed in [19] for X-band applications by using an array structure with a dimension of 156 × 9 mm^2. In [20], a 3D printed corrugated plate antenna with high gain and aperture efficiency was proposed in the work. It is reported that the gain of the antenna is improved with the increment of the number of corrugated structures. The highest gain of 24.2 dB was achieved when 10 corrugations were implemented in the antenna structure. A proximity coupled technique is also being proposed for microstrip patch antennas (PC-MSPA) in S/C/X-band applications as reported in [21]. The prediction of the impedance response was conducted for a two-layer and single-material design structure. As a result, a new prediction model based on an electric equivalent circuit was introduced accordingly. To achieve the acceptable performance of an antenna using 3D electromagnetic simulation software, such as CST, HFSS, FEKO, and ADS, is a very challenging and time-consuming task. To mitigate these limitations, many researchers apply machine learning (ML) and deep learning (DL) approaches to optimize the antenna design, predict the results, such as resonance frequency (f_r), gain, return loss (s_{11}), bandwidth, and so on, and select the antennas for wireless applications [22–29]. Authors in [30] proposed an artificial neural network (ANN)-based microstrip patch antenna where the antenna dimension and resonance frequencies were predicted. However, the accuracy of the predicted results in terms of percentage of error, such as MSE, MAE, and RMSE, was not considered. Moreover, the prediction results of the proposed ANN model were not compared with the other existing ML models to validate the prediction. Another research work was carried out to predict the resonance frequency of patch antennas using ANN in [31]. In this research work, the percentage of error was calculated from the difference between actual value and predicted value divided by the actual value. It is noteworthy that the percentage of error in terms of MSE, MAE, and RMSE was not evaluated. In addition, most of the existing ML-based antenna design research work has not measured the variance score. In this research work, six regression ML models, such as linear regression (LR), random forest regression (RFR), decision tree regression (DTR), Lasso regression, ridge regression (RR), extreme gradient boosting (XGB) regression, and one DL model (CNN), are used to predict the operating frequency of the proposed antenna. Various performance metrics, such as mean square error (MSE), mean absolute

error (MAE), root MSE (RMSE), and variance score are observed to validate the prediction of the f_r using the mentioned models [32].

Recently, a new technique has been explored by using multiple regression algorithms along with convolutional neural networks (CNN) to predict the f_r by using CST electromagnetic (EM) simulation tools. Furthermore, the simulated f_r using CST and ADS and measured f_r is compared with the predicted f_r using the proposed ML algorithms.

The main contributions of this research work are summarized as follows:

i Simulate and analyze the performance of a microstrip patch antenna using CST EM simulation tools.
ii Validate the CST simulation results using ADS simulation software, and the simulated S_{11} is compared with the measured S_{11}.
iii The resonance frequency (f_r) is predicted using six ML regression algorithms and CNN. A comparative study of the different models based on the different predicted results is incorporated.

The remaining sections of this study are organized as follows. Section 2 explains several generic design formulas and the geometrical structure of the proposed antenna and the required performance analysis of the various machine learning algorithms. The results of the necessary simulations and measurements are presented in Section 3 and, consequently, the concluding remarks are highlighted in Section 4.

2. Design Methodology

In microstrip patch antennas, the size and shape of the patch determine the antenna's resonance frequency, bandwidth, return loss, gain, and radiation pattern. Radiation efficiency and resonance frequency are two of the many variables whose values are directly determined by the patch's width and length. The feasible and efficient dimensions (length and width) of a rectangular microstrip antenna can be calculated using the formulae below. Based on the transmission line model, the dimensions of a radiation patch can be calculated using the following equations [33,34]:

$$W = \frac{c}{2f_r}\sqrt{\frac{2}{\epsilon_r + 1}} \tag{1}$$

$$L = \frac{c}{2f_r\sqrt{\epsilon_{eff} + 1}} - 2\Delta L \tag{2}$$

where

$$\Delta L = 0.412h\frac{\epsilon_{eff} + 0.3}{\epsilon_{eff} - 0.258}\left[\frac{\frac{w}{h} + 0.264}{\frac{w}{h} + 0.8}\right] \tag{3}$$

$$\epsilon_{eff} = \frac{\epsilon_r + 1}{2} + \frac{\epsilon_r - 1}{2}\left[1 + 12\frac{h}{w}\right]^{-\frac{1}{2}} \tag{4}$$

and feedline W_0 is evaluated from the input impedance Z_{in}:

$$Z_{in} = \frac{120\pi}{\sqrt{\epsilon_r}\left[\frac{h}{w} + 1.393 + 0.667ln\left(\frac{h}{w} + 1.444\right)\right]} \tag{5}$$

Here, c is the speed at which light travels through a vacuum, (f_r) is the resonance frequency, and ε_r is the relative permittivity (also called the dielectric constant) of the dielectric material. In real life, the fields do not just stay on the patch. The fringing field is a field component that goes beyond the patch's physical limits ($L \times W$). The effective patch width could be calculated using the effective dielectric constant (ε_{reff}) for the width of the patch (W) while considering the influence of the fringing field effect. The effective dielectric constant (ε_{reff}) is determined by the following equation:

$$\epsilon_{eff} = \frac{\epsilon_r + 1}{2} + \frac{\epsilon_r - 1}{2}\left[1 + 12\frac{h}{w}\right]^{-\frac{1}{2}} \tag{6}$$

Here, h is the thickness of dielectric substrate. To account for the influence of the fringing field given a patch length L, both ends of the line must have a length added to them.

$$\frac{\Delta L_{\epsilon_{eff}}}{h} = 0.412h\frac{\left(\epsilon_{eff} + 0.3\right)\left(\frac{w}{h} + 0.264\right)}{\left(\epsilon_{eff} - 0.258\right)\left(\frac{w}{h} + 0.8\right)} \tag{7}$$

The antenna has a total footprint of 28.2 × 23.8 × 1.6 mm^3 with a patch area of 28.2 × 23.8 mm^2. Annealed copper is used as a patch and ground plane material and is matched to the real-world antenna construction material.

FR4 is, rightly, the most commonly used material in PCB construction. Boards from FR4 are robust, water resistant, and provide sound insulation between copper layers that minimize interference and support good signal integrity. This research investigated the feasibility of using the FR-4 substrate for microstrip antennas throughout a wide frequency range (8–12 GHz). The purpose of this investigation was to examine the FR-4 substrate as a potential option for designing an X-band microstrip antenna, aiming to achieve a high degree of agreement between simulated and measured results. Due to its inexpensive cost and widespread availability, FR-4 was selected for this research because it can be utilized for prototyping microstrip antennas. A microstrip feed line with a 50 Ω impedance was used to feed the input signal to the antenna. CST carries out the preliminary design and performance optimization. The dimensional parameters of the proposed MPA are presented in Table 1.

Table 1. Antenna design parameters.

Parameters	Full Form of Parameters	Dimensions (mm)	Parameters	Full Form of Parameters	Dimensions (mm)
L_S	Length of Substrate	23.8	L_f	Length of Feed Line	10
L_G	Length of Ground	28.2	W_f	Width of Feed Line	3
W_G	Width of Ground	9.6	L_i	Length of Inset	5
L_P	Length of Patch	13.8	W_i	Width of Inset	3.6
W_P	Width of Patch	19	M_{tP}	Thickness of patch	0.035
h	Thickness of substrate	1.6	M_t	Thickness of Ground	0.035
W_S	Width of Substrate	28.2	-	-	-

The proposed MPA utilizes FR-4 Epoxy dielectric material, which has a relative permittivity of $\varepsilon_r = 4.4$ and loss tangent of 0.007. The antenna features a rectangle-shaped patch with two inset slot cuts and a partial ground plane with a smaller area than the substrate. The parametric analysis in CST derives the optimal dimensions of insets and ground planes. Optimized dimensions of inset slots in combination with a partial ground plane give an excellent wideband response. Figure 1a,b depict a simulated 3D view; the partial ground plane of the proposed MPA and Figure 2a shows the dimensions of substrate, patch, and feedline of the proposed X-band MPA and Figure 2b depicts the fabricated prototype view

of the proposed wideband MPA that has the capability to satisfy X-band applications requirement.

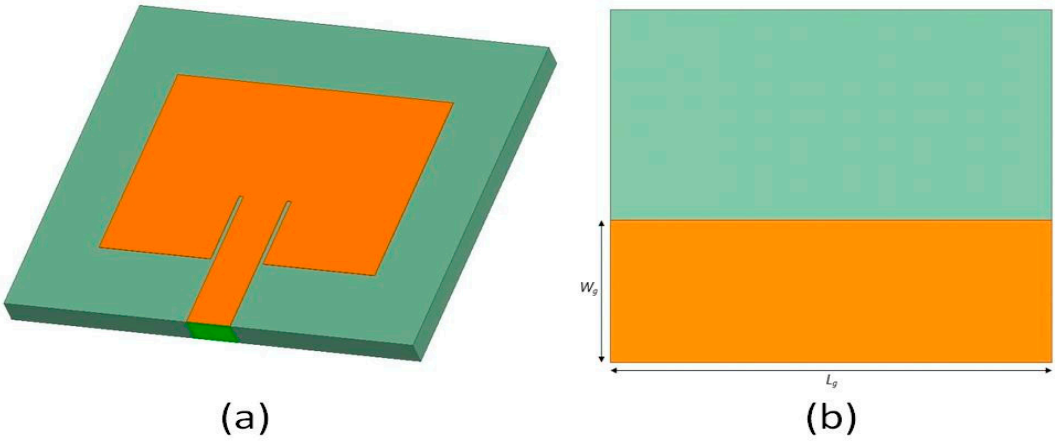

Figure 1. (**a**) Three-dimensional view and (**b**) partial ground plane of the proposed X-band MPA.

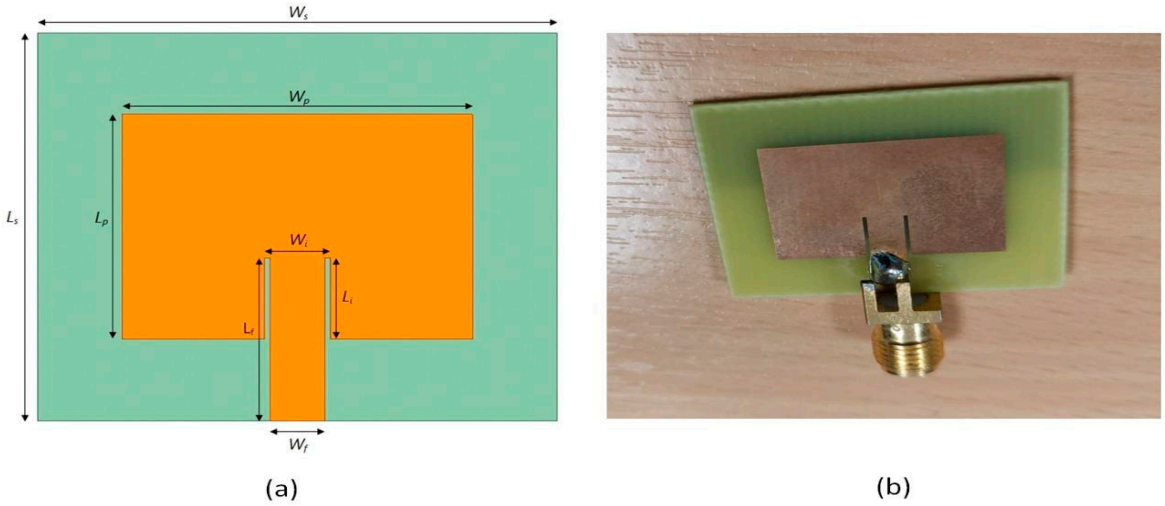

Figure 2. (**a**) Front view of the proposed MPA. (**b**) Fabricated Prototype.

3. Result Analysis of the Proposed MPA

The simulated and measured results of the proposed MPA are discussed in this section. The simulated S_{11} using CST is also compared with the results obtained from the advanced design system (ADS). Finally, different machine learning algorithms are discussed briefly to predict the proposed antenna's resonance frequency.

3.1. Simulated and Measured Results

The simulated and measured S_{11} plot is shown in Figure 3. The simulated and measured S_{11} plot ensures that the proposed MPA will provide satisfactory performance across the whole X-band. Moreover, the S_{11} graph shows that the antenna will be suitable for the entire X-band and a portion of the lower part of the Ku-band. The MPA provides two resonance frequencies of 9 GHz and 13 GHz with return loss magnitudes of S_{11} −35 dB and −18 dB, respectively. The MPA offers a −10 dB impedance bandwidth of 5.8 GHz, ranging from 8.35 GHz to 14.15 GHz. However, the measured return loss graph is slightly different from the simulated return loss graph. It may have occurred because the antenna is excited using a waveguide port during simulation, but practically the antenna is excited using the SMA connector. The connector loss influences the response of the antenna. In addition, the near-field scattering objects, the losses due to the feed connector, and the

coaxial cable also affect the response of the antenna performance. Figure 4 shows that the VSWR is less than 1.5 at both resonance frequencies, ensuring good impedance matching characteristics.

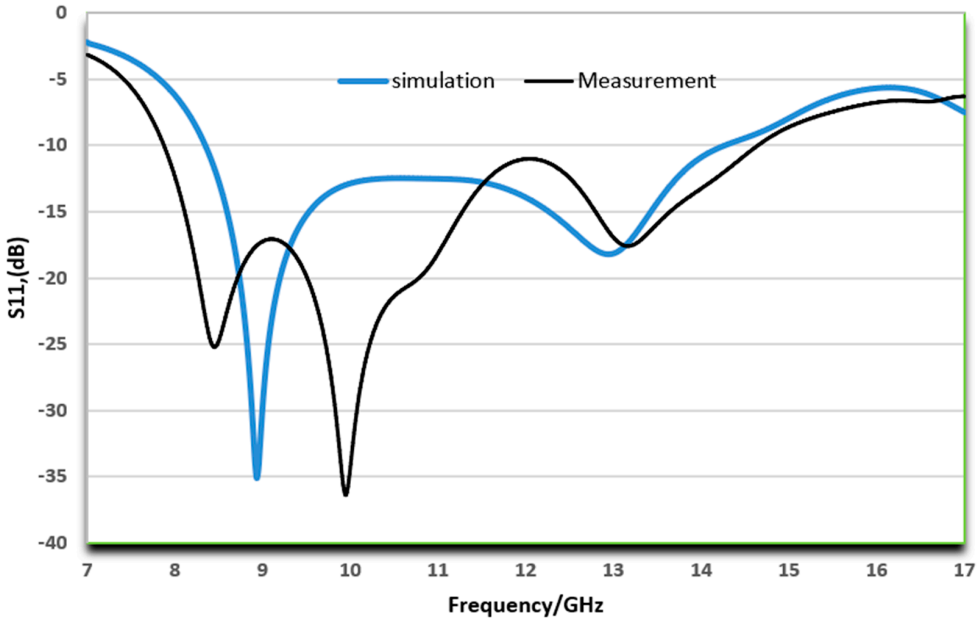

Figure 3. Return loss (S_{11}) vs. frequency plot of the proposed MPA.

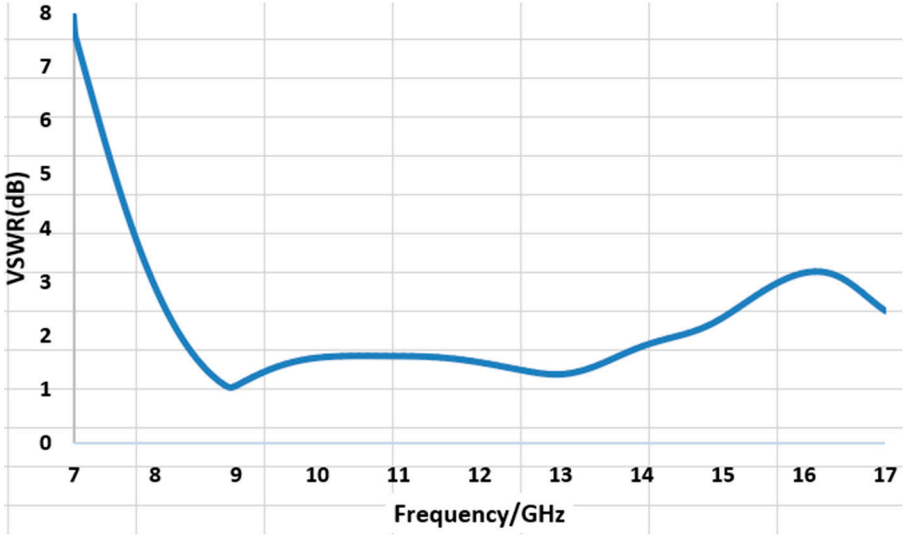

Figure 4. Simulated VSWR of the proposed MPA.

The surface current distribution of the designed MPA indicates that the antenna has the most current in the middle of its length and the least current near its edges, as illustrated in Figure 5. To validate the simulated and measured S_{11}, the equivalent RLC model of the proposed antenna is designed using Agilent ADS software and the resonance frequencies obtained from the RLC equivalent model of the proposed MPA using ADS Agilent software are almost equal to the simulated (using CST) and measured resonance frequencies. In addition, the S_{11} using ADS is −34 dB and −35 dB at both resonance frequencies.

The radiation pattern of the proposed antenna is depicted in Figure 6, which shows the main lobe direction, main lobe magnitude, side lobe level (SLL), and a 3-dB beam width. At the two distinct resonance frequencies, the 3-dB beam width is 148.2 degrees for 9 GHz and 71 degrees for 13 GHz. The SLL at a resonance frequency of 13 GHz is −6.3 dB and at

a frequency of 9 GHz it is −10 dB. Gain is a measurement of the energy delivered to the main beam. The gain vs. frequency curve of the proposed antenna is presented in Figure 7. From the figure, the gain of the microstrip patch antenna varies from 2.2 dB to 6.25 dB in the entire simulated frequency range. The designed antenna gained 4.0614 dB at 9 GHz and 3.4589 dB at 13 GHz.

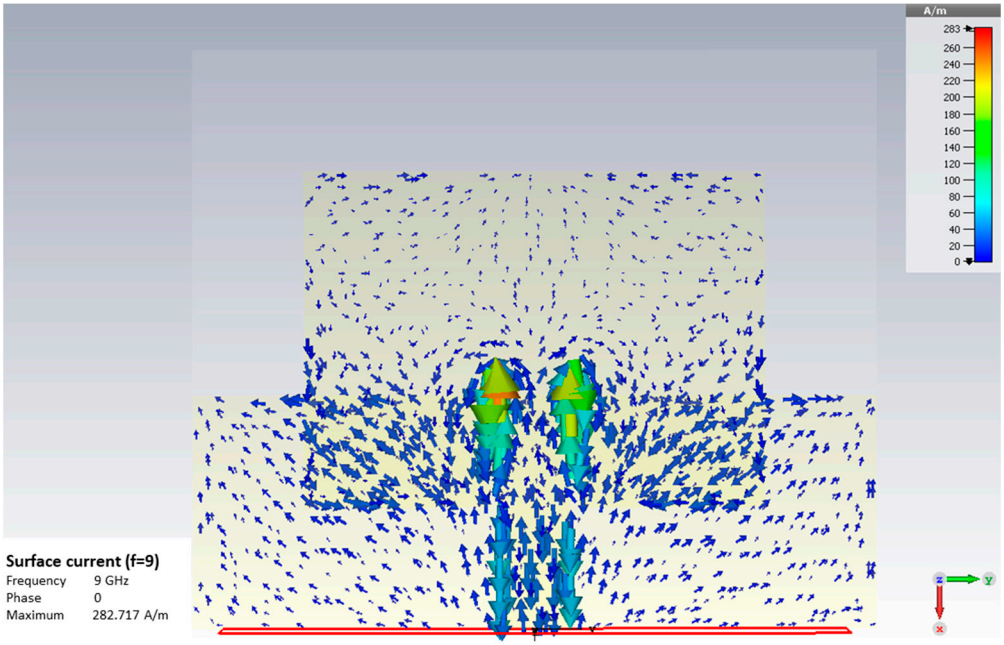

Figure 5. Surface current distribution.

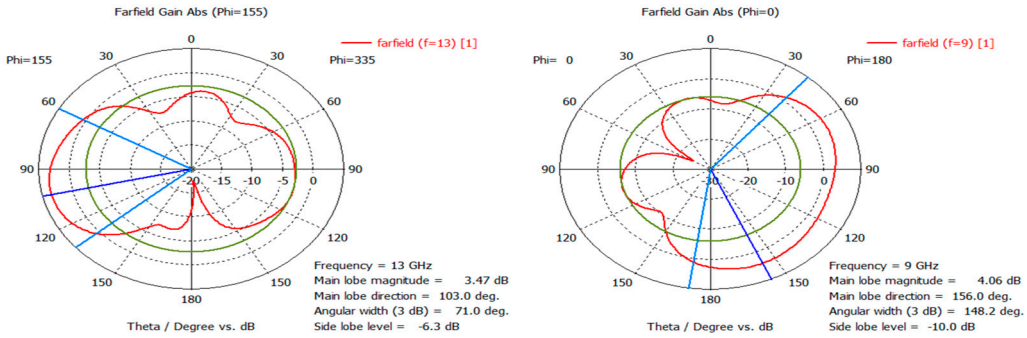

Figure 6. Radiation pattern of the proposed MPA.

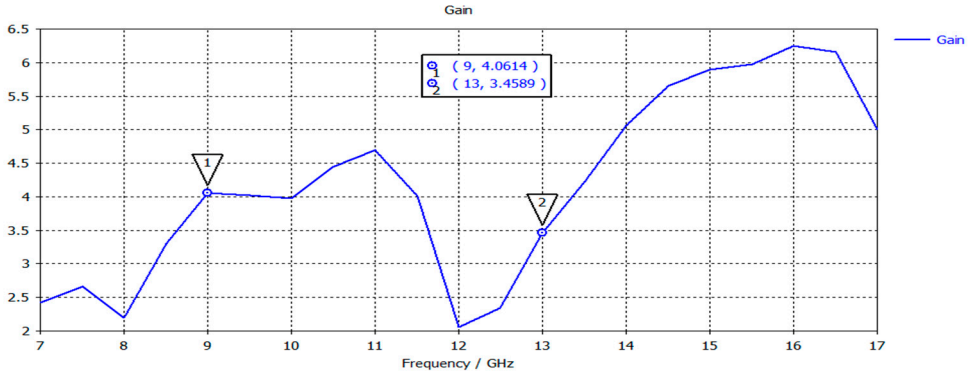

Figure 7. Gain vs. frequency plot of the proposed MPA.

3.2. RLC Lumped Element Extraction and Equivalent Circuit of the Proposed MPA Using ADS

The equivalent RLC model of the proposed MPA using Agilent ADS software is presented in Figure 8. The values of R, L, and C have been chosen so that the equivalent impedance of the designed antenna is reasonably matched with the characteristic impedance (50 Ω) of the transmission line. An optimal impedance match between the antenna and the transmission line is required to transfer maximum power from the input port of the antenna to its antenna structure [35]. For the resonance frequencies of 9 GHz and approximately 13 GHz, resistance $R1 = 52.56\ \Omega$, inductance $L1 = 49.8$ pH, and capacitance $C1 = 6.369$ pF are assigned to the parallel RLC circuit, along with resistance $R2 = 51.88\ \Omega$, inductance $L2 = 135.8$ pH, and capacitance $C2 = 1.10$ pF as presented in Figure 8. As the antenna input port, the input terminal source in ADS is configured as a terminal block (Term is G) with a 50 Ω characteristic impedance and acts as an input port for the antenna. The values of R, L, and C are considered in such a manner that the equivalent circuit impedance is equal to the antenna input port impedance. The impedance matching performance is observed in ADS using the S-parameter block. In the S-parameter block, the intended frequency range is swept from 7 GHz to 17 GHz in 10 KHz increments. The plot of the return loss response (dB (S (1,1)) is chosen for plotting the resonant circuit's output result. The resonant circuit yields a resonant frequency of 9.0 GHz with a return loss of −33 dB, and at 13 GHz with a return loss of -35 dB, as shown in Figure 9.

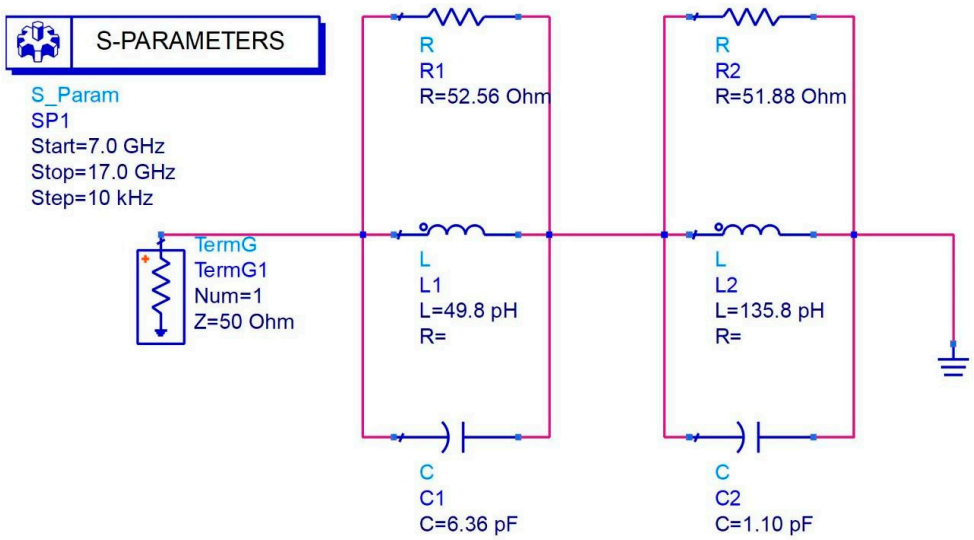

Figure 8. Circuit diagram of a parallel RLC circuit for resonant frequency (refer to CST simulation) using ADS Agilent simulation.

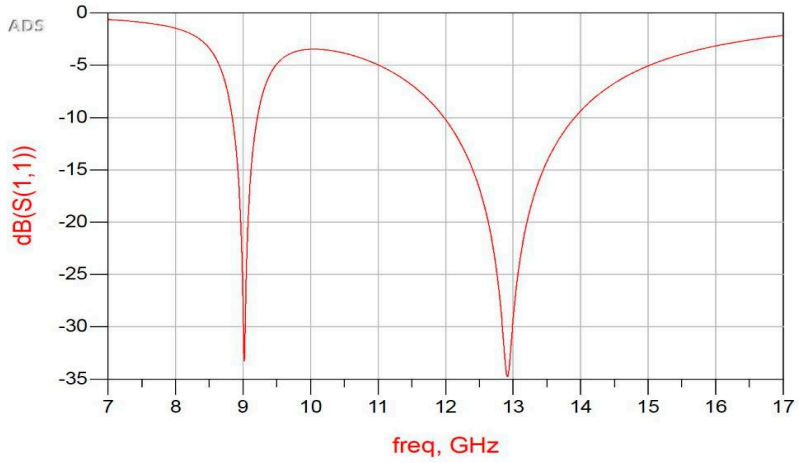

Figure 9. Simulated result using ADS Agilent equivalent circuit.

3.3. Machine Learning-Based Resonance Frequency Prediction

To achieve simplicity in the design of the antenna and predict the antenna performances, different ML and/or DL models are introduced. Using those models, the design and optimization of the antennas are much easier than with the traditional EM simulation tools. In this study, we are investigating and showing a wide variety of regression methods along with convolutional neural networks (CNN). All these algorithms are used to predict the resonance frequency of the proposed MPA. A brief description of the different models that are used for the prediction of resonance frequency is provided in the following subsection.

4. Brief Description of the Learning Models

Machine Learning Models:

Machine learning creates algorithms from data and then uses those algorithms to generate predictions based on other data. Multiple methods, including regression, classification, and deep learning, see heavy rotation in the machine learning toolkit (Neural Network). To solve this problem, we are investigating and showing various regression methods. It is common practice to employ regression when making predictions and forecasts.

Convolutional Neural Network (CNN):

CNN has been proposed for use on one-dimensional data in addition to its widespread application in image recognition and text analysis. In convolutional neural networks, there are three types of layers: input, hidden, and output. Both the input and output layers are activated linearly. However, since neural networks can have multiple hidden layers, their activation functions are often nonlinear. Hidden layers in convolutional neural networks (CNNs) convolve the input and send the result to the next layer [36,37]. Table 2 shows the hyperparameter settings of the CNN model. The CNN architecture is shown in Figure 10.

Table 2. Hyperparameter setting for used CNN.

Hyperparameter	Configuration
Dense layer's activation function	ReLU
Batch size	16
Epoch	100
Optimization function	Adam
Loss	MSE

Linear Regression:

Linear regression is a well-known approach in the fields of statistics and machine learning. This is a mathematical technique used in forecasting or predicting results. A linear regression model aims to establish a correlation between a set of characteristics and a continuous dependent variable [38].

Random Forest Regression:

Classification and regression with random forests involve constructing a set of tree predictors, each of which is built with a random vector that is chosen independently of the input vector. Regression with tree predictor uses numerical values in place of class labels. Random forest regression constructs a tree when using variables at each node [39].

Decision Tree Regression:

Decision tree regression considers an object's qualities and trains a model to predict future data and give useful continuous output. It is a tree structure for quantitatively forecasting the results of the dependent variable [40].

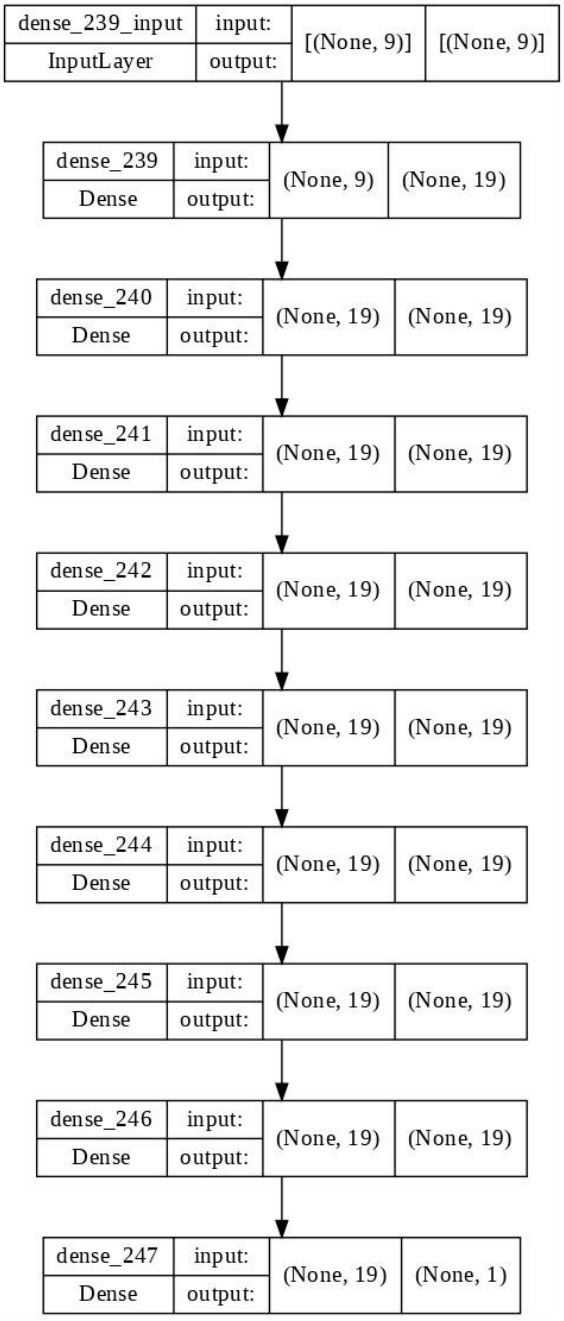

Figure 10. CNN architecture.

Lasso Regression:

Lasso regression is one type of linear regression that employs the shrinkage method. Researchers often turn to lasso regressions for modeling scenarios with many features [41] because of its efficiency in executing feature selection.

Ridge Regression:

A valuable method for analyzing multiple regression on data that exhibits multicollinearity is known as ridge regression. It is a regularization model where an extra variable (tune parameter) is added and optimized to address numerous variables in linear regression [42].

XGB Regression:

When it comes to fixing regression or classification issues, the most efficient method is extreme gradient boosting (XGBoost). This approach uses a gradient boosting framework to make use of decision trees. It provides features that significantly affect the model's efficacy [43].

The data generation flow diagram is shown in Figure 11. There are six regression models, linear regression, random forest regression, decision tree regression (DTR), lasso regression, ridge regression, XGB regression, and CNN, used to predict the resonance frequency. The comparisons between the simulated and the predicted resonance frequencies of the 18 test data samples using DTR and CNN are shown in Tables 3 and 4, respectively

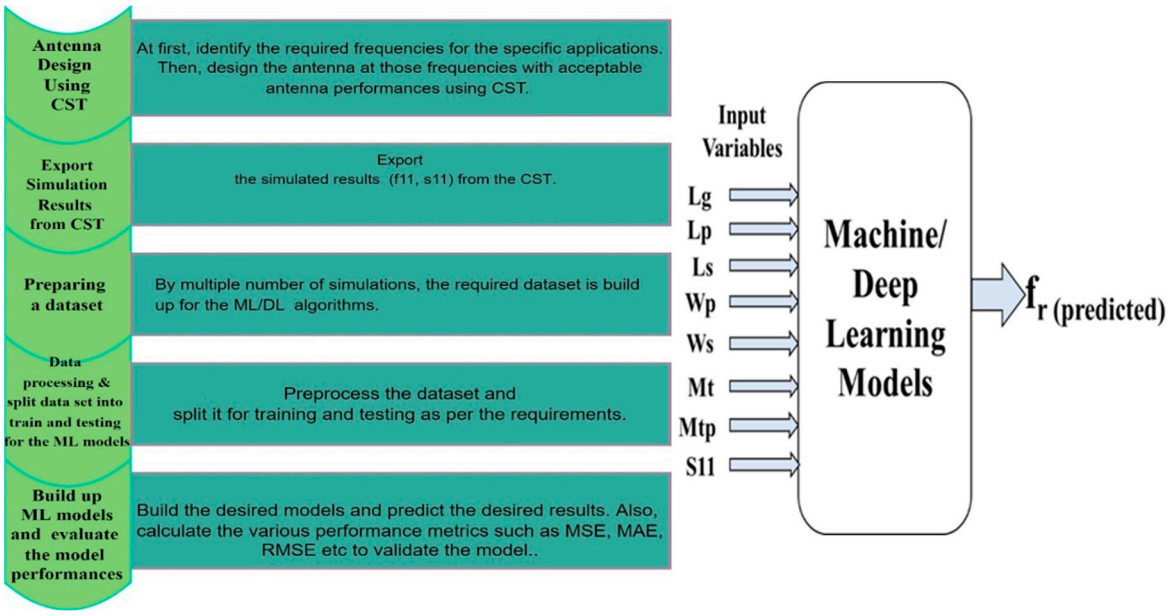

(**a**) (**b**)

Figure 11. (**a**) Flowchart for ML/DL-based antenna results prediction; (**b**) analysis of MPA using ML/DL models.

Table 3. Simulated and predicted resonant frequency comparison of the test set using DTR.

No.	Simulated Frequency (GHz)	Predicted Frequency (GHz)	Error Percentage (%)	No.	Simulated Frequency (GHz)	Predicted Frequency (GHz)	Error Percentage (%)
1	8.1414	8.1113	0.3697	10	9.064	9.0285	0.3917
2	9.0396	9.0285	0.1228	11	9.0296	9.0296	0
3	9.1176	9.0953	0.2446	12	8	8.1526	1.9075
4	9.0507	9.0507	0	13	11.81	11.794	0.1355
5	7.2623	7.2623	0	14	9.1413	9.2296	0.9659
6	9.351	9.3841	0.354	15	11.734	11.634	0.8522
7	11.988	11.794	1.6183	16	11.649	11.794	1.2447
8	8.1487	8.1526	0.0479	17	9	9.0173	0.1922
9	11.865	11.712	1.2895	18	9.0639	9.0753	0.1258

Table 4. Simulated and predicted resonant frequency comparison of the test set using CNN.

No.	Simulated Frequency (GHz)	Predicted Frequency (GHz)	Error Percentage (%)	No.	Simulated Frequency (GHz)	Predicted Frequency (GHz)	Error Percentage (%)
1	8.1414	8.6086	5.73869	10	9.064	9.222	1.74353
2	9.0396	9.225	2.05042	11	9.0296	9.6116	6.44494
3	9.1176	9.2757	1.73436	12	8	8.7789	9.7363
4	9.0507	9.265	2.36726	13	11.81	10.3787	12.11948
5	7.2623	8.7624	20.65657	14	9.1413	9.2286	0.95446
6	9.351	9.7752	4.53594	15	11.734	10.8604	7.44519
7	11.988	10.3457	13.69946	16	11.649	9.7128	16.62076
8	8.1487	8.8375	8.45233	17	9	9.2611	2.90101
9	11.865	10.2844	13.32168	18	9.0639	9.8493	8.6656

Performance Evaluation of the ML Models

Different performance metrics of the ML models are investigated to validate the prediction of the resonance frequency with respect to the simulated and the measured resonance frequency. In this research work, the mean absolute error (MAE), the mean squared error (MSE), the root mean squared error (RMSE), and the variance score are observed as performance indicators of the ML regression models. Predicting errors are computed, and prediction models are assessed using these metrics. The mean absolute error, mean squared error, and root-mean-squared error are well-known scale-dependent measurements based on absolute and squared values [44,45]. The MAE considers the average amount of error over a group of projections but ignores the direction of the mistake, giving less weight to extreme predictions [46]. In [47], the MAE is mathematically formulated as:

$$MAE = \frac{1}{n}\sum_{i=1}^{n}|Pi - Oi| \tag{8}$$

where n = number of errors and $|Pi - Oi|$ = Absolute error.

The MSE is a common statistic used in estimation. The root-mean-squared error (*RMSE*) is used in place of MSE by taking the square root. The root-mean-squared error (*RMSE*) quantifies how far estimates deviate from reality. The definition of *RMSE* is [48]:

$$RMSE = \sqrt{\frac{1}{n}\sum_{i=1}^{n}(Pi - Oi)^2} \tag{9}$$

Another performance indicator is the explained variance score that reflects the error scatter in a data collection. It can be defined as [49]:

$$explained\ variance(y, \hat{y}) = 1 - \frac{Var(y - \hat{y})}{Var(y)} \tag{10}$$

Figure 12 shows that a total of 86 samples were used to predict the resonance frequency of the designed MPA. Among the 86 samples, 68 samples were used to train the models and 18 samples were used to test the models' performance. The number of training samples and the number of sampling data determines the accuracy of the prediction model. The 86 data samples were generated using CST simulation software by varying the different dimensional parameters of the proposed MPA.

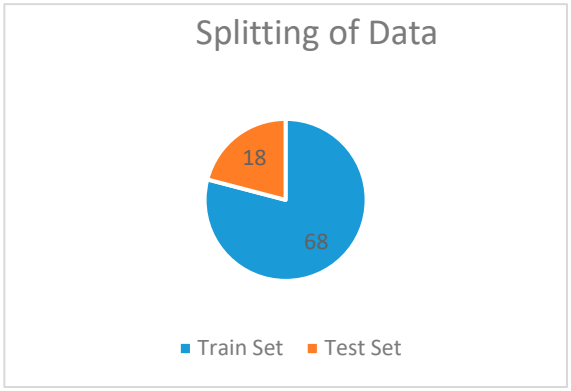

Figure 12. Pie chart for splitting the data set.

Figure 13 shows a heat map plot (correlation matrix) which represents each of the ten attributes of antenna design parameters named Lp, Ls, Lg, Wp, h, Ws, Mtp, Mt, S11, and frequency on the y- and x-axis of the plot. These values represent the input dimensions of the proposed antenna structure, as shown in Table 1 and Figure 2 in the previous section. The maximum correlation occurs at the center of the plot with a value of 1.00. As the point moves away from the maximum line (1.00), the correlation decreases accordingly. In this mapping plot, the correlation value ranges from 0.03 to 0.72.

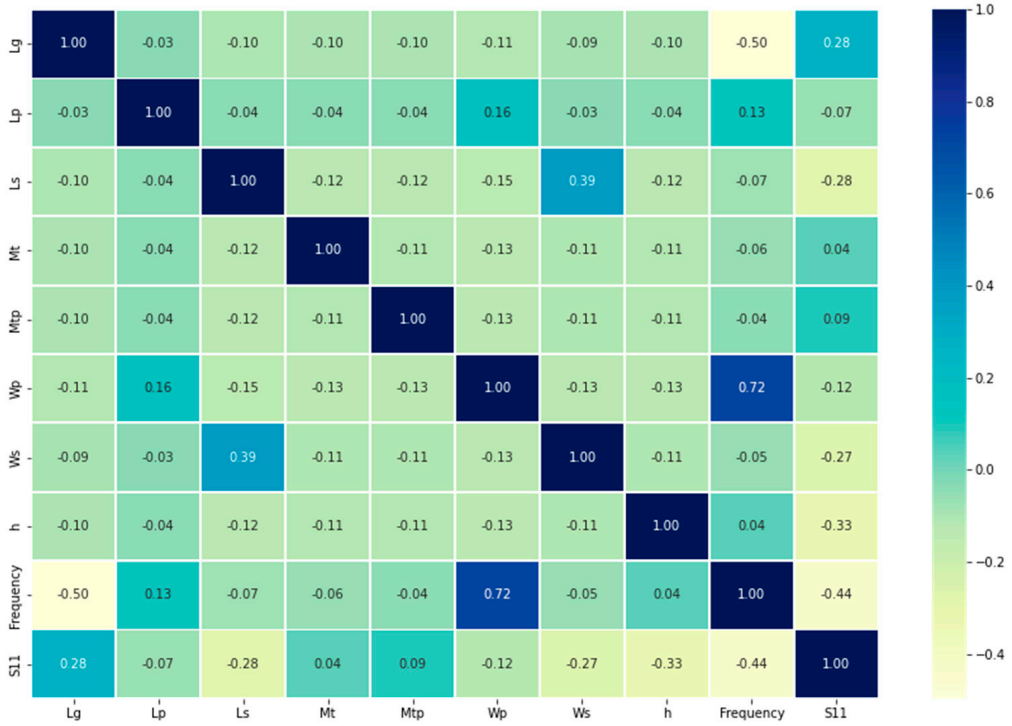

Figure 13. Correction matrix.

Figure 14 shows the simulated vs. predicted frequency of test data samples using DTR and CNN, respectively, for 18 test samples. In the analysis, the frequency tuning ranges from 7 GHz to 12 GHz. It is shown in Figure 14a that there is a small deviation (close to 0) between the actual and predicted frequencies for DTR. Among the 18 test samples, 3 test samples were accurately predicted, with zero percentage of error. In addition, the percentage of error in most cases is less than one. As a result, the predicted result almost perfectly matches the simulated result, as shown in Figure 14a. Somehow, there are deviations for CNN with magnitudes ranging from 0.95446% to 20.65657% as depicted in Figure 14b. It is found that the percentage of predicted errors in CNN is slightly higher

than in DTR. Hence, DTR is selected for better prediction performance as compared to CNN.

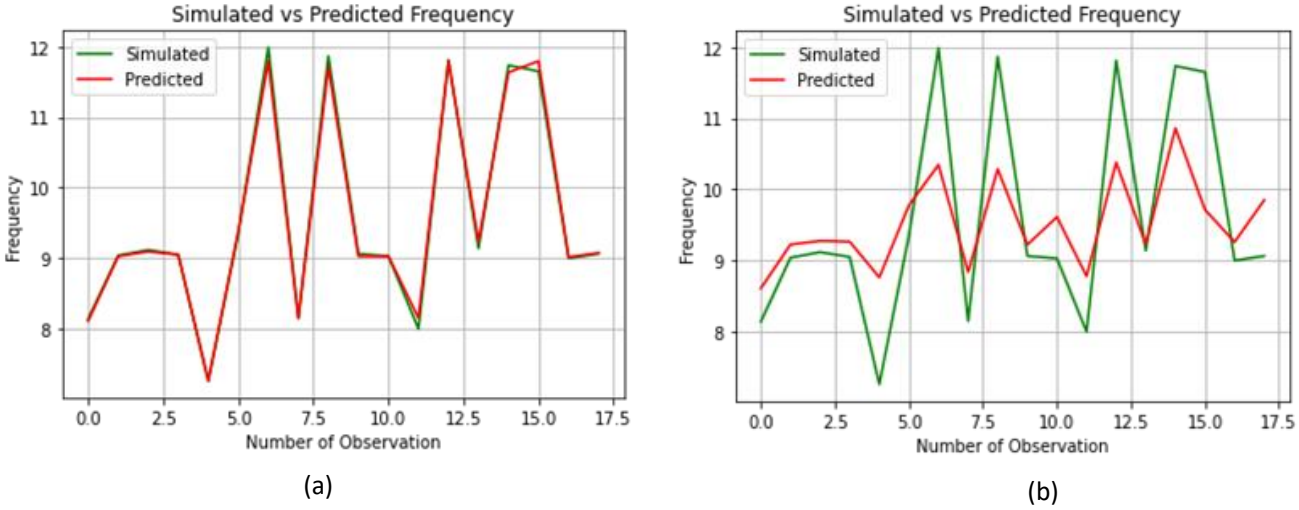

Figure 14. Simulated vs. predicted frequency using (**a**) DTR and (**b**) CNN.

The performance metrics of ML for CNN, linear regression, random forest regression, decision tree regression (DTR), lasso regression, ridge regression, and XGB regression algorithms are tabulated in Table 5. The magnitude values of MAE, MSE, RMSE, and the variant score are evaluated to determine the error performance of each algorithm. It is shown that the DTR model generates a small percentage error for MAE, MSE, RMSE, and the variant score magnitude with values of 5.63%, 0.71%, 8.42%, and 99.68%, respectively. The DTR method has performed better than the rest of the regression models and yields the highest quality results in all four scenarios. It is also shown that the XGB model is considered as a secondary selection, where it generates values of 7.03%, 1.06%, 10.27%, and 99.54%, respectively. It depicts the XGB model, performing close to DTR. Somehow, the performance of the CNN and Lasso models produced lower percentage magnitudes of 76.41%, 92.49%, 96.17%, and 57.62% and 55.01%, 63.25%, 79.53%, and 70.97%, respectively. Hence, they are not good for method selection for proposed research work. The performance comparison for all algorithms viewed in the bar chart is illustrated in Figure 15.

Table 5. The resonant frequency prediction performance of ML algorithms.

Algorithms	MAE	MSE	RMSE	Var Score
CNN	0.7641	0.9249	0.9617	0.5762
Linear Regression	0.5312	0.5226	0.7229	0.7627
Random Forest Regression	0.1261	0.0352	0.1875	0.9848
Decision Tree Regression	0.0563	0.0071	0.0842	0.9968
Lasso Regression	0.5501	0.6325	0.7953	0.7097
Ridge Regression	0.5061	0.5159	0.7183	0.7668
XGB Regression	0.0703	0.0106	0.1027	0.9954

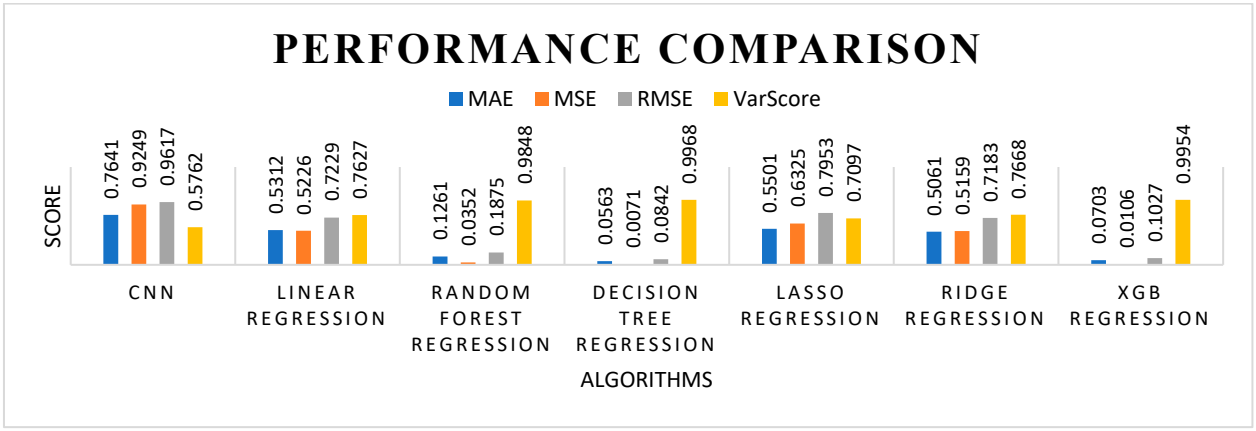

Figure 15. Comparative bar chart for seven algorithms.

5. Conclusions

This article discusses the integration of simulation, measurement, development of the RLC equivalent circuit model, and applying machine learning approaches to evaluate the performance of the proposed antenna. In terms of frequency, the designed antenna supports the whole X-band as well as some portions of the Ku-band. The prototype was built and analyzed to confirm the intended performance. In addition, the RLC equivalent model of the proposed MPA designed with the ADS Agilent software yields resonance frequencies nearly identical to those generated by simulation (with CST) and measurement. Furthermore, six machine learning and one deep learning (CNN) algorithm have been developed to determine the resonant frequency of the MPA. When the predicted and simulated resonant frequencies are compared, it is observed that they are almost identical. Different performance metrics, such as MAE, MSE, RMSE, and variance scores, are calculated to validate the prediction using the learning algorithms. These metrics are obtained through the process of computing the results of the prediction. The predicted results show that the error performances of the decision tree regression model are comparatively better than other models. The MAE, MSE, RMSE, and variance scores (in percentage) of the DTR model are 5.63, 0.71, 8.42, and 99.68, respectively. The XGB model (MAE = 7.03%, MSE = 1.06%, RMSE = 10.27%, and var score = 99.54%) performs better than the other learning models that were introduced in this study, except DTR. The performance of the deep learning model (CNN) is slightly lower than the presented regression models, which may have occurred due to the inadequate number of data samples for the CNN model. Despite the fact that the proposed MPA has two resonant frequencies, we have only predicted one (9 GHz) using ML models. In addition, the designed MPA has a lower gain of 4.06 dB at 9 GHz and 3.46 dB at 13 GHz. The measured resonance frequency range (7.90 GHz to 14.6 GHz) does not quite correspond to the predicted resonance frequency range (8.35 GHz to 14.25 GHz). In the future, we will generate an adequate number of data samples to achieve better results using DL models, such as CNN, and predict the multiple frequencies for a multiband antenna. Furthermore, we will develop the ML models to predict the return loss, gain, length, and width of the proposed antenna. Moreover, we will ensure better impedance matching between the proposed MPA and the SMA connector so that the simulated and measured frequencies are completely matched. Finally, it can be concluded that the simulated, measured, and predicted results ensure the reliability of the proposed antenna in the whole X-band and part of Ku-band applications.

Author Contributions: M.A.H. and N.S. presented the idea, performed the experiments, prepared the manuscript and visualization, N.S.S.S. prepared funding acquisition. M.A.R. and L.C.P. prepared the data curation and formal analysis, M.N.H. and M.I. described the investigation and methodology. M.A.Z. contributed to the supervision of the research work. G.E.M.A. and A.H.S. contributions

include software development, resources, and validation. M.H. and R.P. contributed to writing and reviewing. All authors have read and agreed to the published version of the manuscript.

Funding: Regarding software simulation, this research was sponsored by INTI International University, Malaysia, and they sponsored this research work from the beginning till publication.

Institutional Review Board Statement: Not applicable.

Informed Consent Statement: Not applicable.

Data Availability Statement: Not applicable.

Acknowledgments: The author wishes to extend his sincere thanks to the support of the Centre of Graduate Studies, Universitiy Teknologi, PETRONAS, Malaysia, and the Faculty of Data Science and Information Technology at INTI International University, Malaysia, for providing the state-of-the-art research facilities to carry on this work. In addition, the author is also thankful for the support provided by the collaborators from Condition Monitoring System, National Center of Robotics and Automation, Mehran University of Engineering and Technology, Jamshoro, Sindh, Pakistan. The entire project was sponsored by the Faculty of Data Science and Information Technology, INTI International University, Malaysia, for the necessary results.

Conflicts of Interest: The authors declare no conflict of interest.

References

1. Paul, L.C.; Ali, H.; Sarker, N.; Mahmud, Z.; Azim, R.; Islam, M.T. A Wideband Rectangular Microstrip Patch Antenna with Partial Ground Plane for 5G Applications. In Proceedings of the 2021 Joint 10th International Conference on Informatics, Electronics & Vision (ICIEV) and 2021 5th International Conference on Imaging, Vision & Pattern Recognition (icIVPR), Kitakyushu, Japan, 16–20 August 2021.
2. Kannadhasan, S.; Nagarajan, R. Performance Improvement of S-shaped for Wireless Communication. In *Electronic Systems and Intelligent Computing*; Springer: Singapore, 2022; pp. 15–22.
3. Chowdhury, S.G.; Arefin, M.S.; Faisal, M.M.A. Design Simulation and Analysis of a Dual Band Microstrip Patch Antenna for GPS and WLAN Applications. 2021. Available online: http://dspace.iiuc.ac.bd:8080/xmlui/handle/123456789/3105 (accessed on 10 August 2022).
4. Le, D.; Ahmed, S.; Ukkonen, L.; Björninen, T. A Small All-Corners-Truncated Circularly Polarized Microstrip Patch Antenna on Textile Substrate for Wearable Passive UHF RFID Tags. *IEEE J. Radio Freq. Identif.* **2021**, *5*, 106–112. [CrossRef]
5. Paul, L.C.; Sarkar, A.K.; Haque, A.; Miah, P.; Ghosh, P.M.; Islam, R. Investigation of the dependency of an inset feed rectangular patch antenna parameters with the variation of notch width for WiMax applications. In Proceedings of the 2018 Second International Conference on Electronics, Communication and Aerospace Technology (ICECA), Coimbatore, India, 29–31 March 2018.
6. Huang, G.S.; Li, S.J.; Li, Z.Y.; Liu, X.B.; Di, L.R.J.; Cao, X.Y. Coding-Feeding Metasurface for Diffusion and Dual-Band Emission. *Adv. Theory Simul.* **2022**, *5*, 2200006. [CrossRef]
7. Shi, C.; Zou, J.; Gao, J.; Liu, C. Gain Enhancement of a Dual-Band Antenna with the FSS. *Electronics* **2022**, *11*, 2882. [CrossRef]
8. Muntoni, G.; Montisci, G.; Casula, G.A.; Chietera, F.P.; Michel, A.; Colella, R.; Catarinucci, L.; Mazzarella, G. A curved 3-D printed microstrip patch antenna layout for bandwidth enhancement and size reduction. *IEEE Antennas Wirel. Propag. Lett.* **2020**, *19*, 1118–1122. [CrossRef]
9. Bansal, A.; Gupta, R. A review on microstrip patch antenna and feeding techniques. *Int. J. Inf. Technol.* **2020**, *12*, 149–154. [CrossRef]
10. Fouany, J.; Thevenot, M.; Arnaud, E.; Torres, F.; Menudier, C.; Monediere, T.; Elis, K. New concept of telemetry X-band circularly polarized antenna payload for cubesat. *IEEE Antennas Wirel. Propag. Lett.* **2017**, *16*, 2987–2991. [CrossRef]
11. Khac, K.N.; Phong, N.D.; Manh, L.H.; Le Trong, T.A.; Le Huu, H.; Hien, B.T.T.; Chien, D.N. A design of circularly polarized array antenna for X-band cubesat satellite communication. In Proceedings of the 2018 International Conference on Advanced Technologies for Communications (ATC), Ho Chi Minh City, Vietnam, 18–20 October 2018; pp. 53–56.
12. Ganaraj, G.; Kumar, C.; Kumar, V.S. High gain circularly polarized resonance cavity antenna at X-band. In Proceedings of the 2017 IEEE International Conference on Antenna Innovations & Modern Technologies for Ground, Aircraft and Satellite Applications (iAIM), Bangalore, India, 24–26 November 2017; pp. 1–5.
13. Trentini, G.V. Partially reflecting sheet arrays. *IRE Trans. Antennas Propag.* **1956**, *AP-4*, 666–671. [CrossRef]
14. Asaadi, M.; Sebak, A. Gain and bandwidth enhancement of 2 × 2 square dense dielectric patch antenna arrays using a Holey superstrate. *IEEE Antennas Wirel. Propag. Lett.* **2017**, *16*, 1808–1811.
15. Razi, Z.M.; Rezaei, P. Fabry–Perot cavity antenna based on capacitive loaded strips superstrate for X-band satellite communication. *Adv. Radar Syst. J.* **2013**, *2*, 26–30.
16. Gupta, R.; Mukherjee, J. Effect of superstrate material on a high-gain antenna using array of parasitic patches. *Microw. Opt. Technol. Lett.* **2010**, *52*, 82–88. [CrossRef]

17. Orr, R.; Goussetis, G.; Fusco, V. Design method for circularly polarized Fabry–Perot cavity antennas. *IEEE Trans. Antennas Propag.* **2014**, *62*, 19–26. [CrossRef]
18. Rahman, M.N.; Islam, M.T.; Misran, N.; Samsuzzaman, M. A tuning fork-shaped microstrip patch antenna for X-band satellite and radar applications. In Proceedings of the 2017 6th International Conference on Electrical Engineering and Informatics (ICEEI), Langkawi, Malaysia, 25–27 November 2017; pp. 1–2.
19. Ogurtsov, S.; Koziel, S. A conformal circularly polarized series-fed microstrip antenna array design. *IEEE Trans. Antennas Propag.* **2019**, *68*, 873–881. [CrossRef]
20. Alkaraki, S.; Gao, Y.; Stremsdoerfer, S.; Gayets, E.; Parini, C.G. 3D printed corrugated plate antennas with high aperture efficiency and high gain at X-band and Ka-band. *IEEE Access* **2020**, *8*, 30643–30654. [CrossRef]
21. Ccoillo-Ramos, N.R.; Aboserwal, N.; Qamar, Z.; Salazar-Cerreno, J.L. Improved Analytical Model for a Proximity Coupled Microstrip Patch Antenna (PC-MSPA). *IEEE Trans. Antennas Propag.* **2021**, *69*, 6244–6252. [CrossRef]
22. Kim, J.H.; Choi, S.W. A Deep Learning-Based Approach for Radiation Pattern Synthesis of an Array Antenna. *IEEE Access* **2020**, *8*, 226059–226063. [CrossRef]
23. El Misilmani, H.M.; Naous, T.; Al Khatib, S.K. A review on the design and optimization of antennas using machine learning algorithms and techniques. *Int. J. RF Microw. Comput.-Aided Eng.* **2020**, *30*, e22356. [CrossRef]
24. Bang, J.; Kim, J.H. Predicting Power Density of Array Antenna in mmWave Applications with Deep Learning. *IEEE Access* **2021**, *9*, 111030–111038. [CrossRef]
25. Zheng, B.; Zhang, H. Deep Learning Based Multi-layer Metallic Metasurface Design. In Proceedings of the IEEE International Symposium on Antennas and Propagation, Montreal, QC, Canada, 5–10 July 2020; pp. 2049–2050.
26. Misilmani, H.M.E.; Naous, T. Machine Learning in Antenna Design: An Overview on Machine Learning Concept and Algorithms. In Proceedings of the 2019 International Conference on High Performance Computing & Simulation (HPCS), Dublin, Ireland, 15–19 July 2019; pp. 600–607.
27. Erricolo, D.; Chen, P.-Y.; Rozhkova, A.; Torabi, E.; Bagci, H.; Shamim, A.; Zhang, X. Machine Learning in Electromagnetics: A Review and Some Perspectives for Future Research. In Proceedings of the 2019 International Conference on Electromagnetics in Advanced Applications (ICEAA), Granada, Spain, 9–13 September 2019; pp. 1377–1380.
28. Yao, H.M.; Li, M.; Jiang, L. Applying Deep Learning Approach to the Far-Field Subwavelength Imaging Based on Near-Field Resonant Metalens at Microwave Frequencies. *IEEE Access* **2019**, *7*, 63801–63808. [CrossRef]
29. Wu, Q.; Cao, Y.; Wang, H.; Hong, W. Machine-learning-assisted optimization and its application to antenna designs: Opportunities and challenges. *China Commun.* **2020**, *17*, 152–164. [CrossRef]
30. Kushwah, V.S.; Tomar, G.S. Design and analysis of microstrip patch antennas using artificial neural network. In *Trends in Research on Microstrip Antennas*; IntechOpen: London, UK, 2017; p. 55.
31. Soni, M.; Sharma, K.; Pandey, G.P.; Gupta, S.K. Resonant Frequency Prediction of Patch Antenna in the Presence of Inserted Airgap Using Machine Learning. In *Advances in Smart Communication and Imaging Systems*; Springer: Singapore, 2021; pp. 353–361.
32. Aoad, A. Design and manufacture of a multiband rectangular spiral-shaped microstrip antenna using EM-driven and machine learning. *Elektron. Ir Elektrotechnika* **2021**, *27*, 29–40. [CrossRef]
33. Balanis, C.A. *Antenna Theory: Analysis and Design*; John Wiley & Sons: Hoboken, NJ, USA, 2015.
34. Barthia, P.; Rao, K.V.S.; Tomar, R.S. *Millimeter Wave Microstrip and Printed Circuit Antenna*; Artech House: Boston, MA, USA, 1991.
35. Pozar, D.M. *Microwave Engineering*; John Wiley & Sons: Hoboken, NJ, USA, 2011.
36. Jernelv, L.; Hjelme, D.R.; Matsuura, Y.; Aksnes, A. Convolutional neural networks for classification and regression analysis of one-dimensional spectral data. *arXiv* **2020**, arXiv:2005.07530.
37. Kıymık, E.; Erçelebi, E. Metamaterial Design with Nested-CNN and Prediction Improvement with Imputation. *Appl. Sci.* **2022**, *12*, 3436. [CrossRef]
38. Manasa, J.; Gupta, R.; Narahari, N.S. Machine learning based predicting house prices using regression techniques. In Proceedings of the 2020 2nd International Conference on Innovative Mechanisms for Industry Applications (ICIMIA), Bangalore, India, 5–7 March 2020.
39. Singh, B.; Sihag, P.; Singh, K. Modelling of impact of water quality on infiltration rate of soil by random forest regression. *Model. Earth Syst. Environ.* **2017**, *3*, 999–1004. [CrossRef]
40. Rathore, S.S.; Kumar, S. A decision tree regression-based approach for the number of software faults prediction. *ACM SIGSOFT Softw. Eng. Notes* **2016**, *41*, 1–6. [CrossRef]
41. Madhuri, C.H.R.; Anuradha, G.; Pujitha, M.V. House price prediction using regression techniques: A comparative study. In Proceedings of the 2019 International Conference on Smart Structures and Systems (ICSSS), Chennai, India, 14–15 March 2019.
42. Israni, D.; Masalia, K.; Khasgiwal, T.; Tolani, M.; Edinburgh, M. Crop-yield prediction and crop recommendation system. *SSRN Electron. J.* **2022**. [CrossRef]
43. Torres-Barrán, A.; Alonso, Á.; Dorronsoro, J.R. Regression tree ensembles for wind energy and solar radiation prediction. *Neurocomputing* **2019**, *326–327*, 151–160. [CrossRef]
44. Kumar, R.; Kumar, P.; Kumar, Y. Time series data prediction using IOT and machine learning technique. *Procedia Comput. Sci.* **2020**, *167*, 373–381. [CrossRef]
45. Choo, J.; Pho TH, A.; Kim, Y.H. Machine Learning Technique to Improve an Impedance Matching Characteristic of a Bent Monopole Antenna. *Appl. Sci.* **2021**, *11*, 10829. [CrossRef]

46. Harimurti, R.; Yamasari, Y.; Ekohariadi; Munoto; Asto, B.I.G.P. Predicting student's psychomotor domain on the vocational senior high school using linear regression. In Proceedings of the 2018 International Conference on Information and Communications Technology (ICOIACT), Yogyakarta, Indonesia, 6–7 March 2018.
47. Chai, T.; Draxler, R.R. Root means square error (RMSE) or mean absolute error (MAE)? Arguments against avoiding RMSE in the literature. *Geosci. Model Dev.* **2014**, *7*, 1247–1250. [CrossRef]
48. Willmott, C.J.; Matsuura, K. Advantages of the mean absolute error (MAE) over the root mean square error (RMSE) in assessing average model performance. *Clim. Res.* **2005**, *30*, 79–82. [CrossRef]
49. Weiming, J.M. Mastering Python for Finance—Second Edition. O'Reilly Online Learning. Available online: https://www.oreilly.com/library/view/mastering-python-for/9781789346466/d1ac368a-6890-45eb-b39c-2fa97d23d640.xhtml (accessed on 21 August 2022).